American Mineralogist, Volume 89, pages 941–949, 2004

Hydrogen solubility and speciation in natural, gem-quality chromian diopside

GEOFFREY D. BROMILEY,[1,*] HANS KEPPLER,[2] CATHERINE MCCAMMON,[1] FIONA A. BROMILEY,[1] AND STEVEN D. JACOBSEN[1]

[1]Bayerisches Geoinstitut, Universität Bayreuth, D-95440 Bayreuth, Germany
[2]Institut für Geowissenschaften, Universität Tuebingen, D-72074 Tübingen, Germany

ABSTRACT

A new technique for performing long duration (up to 300 hours) high-pressure annealing experiments under water-saturated conditions has been developed. This technique has been used to investigate water-solubility and speciation in natural, gem-quality chromian diopside. Capsule design for the technique is a variant of the double-capsule technique, and relies on the use of a semi-permeable Pt membrane, which permits free hydrogen diffusion into samples, but protects samples from reacting with buffer mixtures. The investigation of a natural single crystal of chromian diopside revealed a very unusual annealing behavior: water contents increase sharply after a short annealing period and then decrease slowly to some metastable equilibrium value. The main process that takes place during the annealing experiments is hydrogen diffusion coupled with Fe^{3+} reduction. This essentially reverses the main mechanism for hydrogen loss from mantle samples during exhumation, and the technique therefore provides sample-specific information on original water contents. Absorption bands at 3646 and 3434 cm^{-1} in IR spectra from annealed samples suggest two main mechanisms for hydrogen incorporation in the diopside sample: (1) incorporation of hydrogen onto the O2 site, with vibration of the OH dipole in the direction of a nearby O3 site (along the edge of an M2 site), and (2) incorporation of hydrogen onto the O2 site with vibration of the OH dipole toward a nearby O1 site (along a shared M1–M2 edge) or O2 site (along the edge of an M1 site). The ratio of peak heights between the absorption bands at 3646 and 3434 cm^{-1} is independent of water fugacity but dependent on oxygen fugacity, and appears to provide a measure of the redox state "frozen" into the sample. This ratio could be used to determine whether pyroxenes from upper-mantle xenoliths had experienced concurrent hydrogen-loss and oxidation during exhumation.

INTRODUCTION

Considerable effort has been focused over the last two decades on investigating water incorporation in nominally anhydrous minerals (NAMs). Most of the phases thought to constitute the Earth's mantle have been shown to contain trace amounts of water in the form of structurally bound hydrogen, usually associated with point defects in mineral structures (Bell and Rossman 1992; Ingrin and Skogby 2000). Even though water contents in such phases are much lower than in hydrous minerals, ranging from hundreds to thousands of ppm H_2O by weight (Ingrin and Skogby 2000), water incorporation in NAMs could provide a mechanism for storing significant quantities of water in the Earth's mantle. In addition, water incorporation in NAMs may provide a mechanism for storing water in subducting oceanic lithosphere beyond the stability fields of common hydrous phases. Determination of water solubility in minerals stable in subducting oceanic lithosphere is vital for understanding the capacity for subducting slabs to act as repositories for water, and elucidating an important part of the internal water cycle of the Earth. Examination of ultrahigh pressure (UHP) terrains can provide us with important constraints in determining which minerals may play a role in terms of water storage during subduction of oceanic lithosphere. The clinopyroxene omphacite, a diagnostic mineral and one of the main constituents of UHP eclogites, has been shown to be capable of storing up to several thousand ppm H_2O (Skogby et al. 1990; Smyth et al. 1991; Katayama and Nakashima 2003; Terry et al. 2003). Omphacite is expected to be stable over the entire *P-T* range of subducting slabs in the upper-mantle (Green et al. 2000; Schmidt 1993), and could, therefore, transport significant amounts of water beyond the depths of sub-arc magmatism.

Omphacites can be considered a solid-solution between jadeite ($NaAlSi_2O_6$) and diopside ($CaMgSi_2O_6$) end-members, with significant amounts of additional end-members such as $NaFe^{3+}Si_2O_6$ (aegirine), $CaAl_2SiO_6$ (Ca-Tschermak), $CaFe^{2+}Si_2O_6$ (hedenbergite), and $Ca_{0.5}\square_{0.5}AlSi_2O_6$ (Ca-Eskola component) (see Cameron and Papike 1981; Rossi et al. 1983 for general reviews). Under upper-mantle conditions, omphacites are expected to have the *C*2/*c* structure, with two distinct octahedral sites, a regular M1 site and a more distorted M2 site. Smyth et al. (1991) demonstrated that high water contents in natural omphacites were related to low cation totals (expressed as a significant Ca-Eskola component), and proposed that hydrogen incorporation is related to vacancies at M2 sites. A positive correlation of vacancy content with amount of structurally incorporated water was verified by Terry et al. (2003), who recalculated original water contents and compositions of omphacites from Western Norway which had exsolved quartz and hornblende. Exsolution of silica from UHP omphacites has been noted in several UHP eclogitic terrains

* E-mail: geoffrey.bromiley@uni-bayreuth.de

(Schmädicke and Müller 2000; Zhang and Liou 1999; Zhang et al. 1997). Experimental investigations (Gasparik 1986; Malinovskaya et al. 1991) have also demonstrated that high vacancy concentrations in pyroxenes are likely to be stabilized under upper-mantle conditions. An increase in the vacancy concentration of omphacite would be expected to lead to an increase in the capacity of omphacite to incorporate water during subduction.

Rates of hydrogen diffusion in pyroxenes have been experimentally determined by Hercule and Ingrin (1999), Stalder and Skogby (2003), and Woods et al. (2000). The order of magnitude of these values indicates that pyroxenes from exhumed UHP terrains are likely to have undergone extensive re-equilibration, and measured water contents are likely to be much lower than original values at peak metamorphic conditions. Values of original water content calculated using the method of Terry et al. (2003) are also likely to be lower than saturation because water loss from the samples cannot be excluded. Therefore, in order to accurately determine water solubility in omphacites and other UHP phases, high-pressure experiments are required. Water solubility in several mantle phases as a function of pressure has been experimentally determined using synthesis experiments (e.g., Kohlstedt et al. 1996; Withers et al. 1998; Bolfan-Casanova et al. 2000; Rauch and Keppler 2002; Bromiley and Keppler 2004). However, despite the possible importance of water incorporation in omphacite, no experimental investigations of water solubility have been conducted. This is largely because of the complex crystal chemistry of omphacite and the difficulties involved with synthesizing large, homogeneous, crack- and inclusion-free crystals needed for investigating hydrogen incorporation using Fourier-Transform Infrared (FTIR) spectroscopy or secondary ion mass spectrometry (SIMS). Water solubility in jadeite and in some Na-rich pyroxenes was experimentally investigated by Bromiley and Keppler (2004). By comparing experimental results with data from investigations of water incorporation in natural omphacite, Bromiley and Keppler (2004) demonstrated that jadeite provides a good model for understanding hydrogen incorporation in omphacite, but noted experimental difficulties in synthesizing more complex omphacitic compositions. One alternative to direct synthesis experiments is to conduct annealing experiments. Lu and Keppler (1997) investigated water solubility in pyrope up to 10 GPa by conducting annealing experiments with natural pyrope-rich garnet crystals from the Dora Maira complex. In such experiments, samples of natural crystals are placed in sealed capsules with a buffer mixture (to buffer the activities of silica and other species), oxygen buffer and water. Problems can often occur due to reaction of the sample with the buffer mixture, placing a time limit on the duration of experiments. In many instances, it is difficult to demonstrate that equilibrium has been attained. Rauch and Keppler (2002) noted difficulties in attaining equilibrium for annealing experiments on natural pyroxenes.

In order to accurately determine water solubility in pyroxenes under UHP conditions, a novel method for performing long-duration (up to hundreds of hours), high-pressure annealing experiments on natural crystals under water-saturated conditions has been developed. The technique has been used to investigate hydrogen solubility and speciation in a natural chromian diopside (hereafter referred to as Cr-diopside).

EXPERIMENTAL METHODS

The starting material for all experiments was a large single crystal with composition $Ca_{0.969}Mg_{0.97}Fe_{0.036}Cr_{0.013}Al_{0.007}Na_{0.025}Si_{1.987}O_{6.00}$ from Inagli, Yakutia, Russia. The sample was a several cm diameter, dark green subhedral crystal. The crystal was orientated using an X-ray precession camera and $1 \times 2 \times 3$ mm blocks were cut and polished, with edges parallel to the **a**, **b**, and **c*** axes, respectively. No evidence for zoning or variation in composition or water content between samples was noted. Starting water contents of the samples were 95 ppm H_2O by weight (details of water content calculations are given below).

A novel method for annealing samples under water-saturated conditions at high-pressure was used. All experiments were performed using a piston-cylinder apparatus. However, the same method could also be adapted for performing experiments at higher pressures using multi-anvil apparatus with 18M or larger assemblies. The technique is a variation of the "double-capsule" technique, and relies on the use of a semi-permeable platinum membrane. Blocks of samples were loaded into 0.1 mm thick, 3.0 mm diameter Pt capsules with 1–2 wt% liquid H_2O. The capsules were welded shut and then placed in a hydrothermal vessel and slowly pressurized to 0.2 GPa. The effect of pressurization was to "shrink-fit" the platinum capsule around the sample, effectively producing a thin Pt "jacket." The samples were then loaded into 10 mm long, 5 mm diameter 90%Pt5%Rh capsules with a hydroxide-oxide mix with the same bulk composition as the Cr-diopside crystals, a Ni-NiO buffer, and approximately 20 wt% liquid H_2O. The capsules were then welded shut. A cross-section of the double-capsule assembly is shown in Figure 1a. The samples were loaded into 0.75″ (0.5 to 1.5 GPa) or 0.5″ (2.0 to 4.0 GPa) piston-cylinder sample assemblies (Fig. 1b). The capsules were surrounded by pyrophyllite sleeves to reduce water loss during the long duration experiments. At elevated pressures and temperatures, the piston-cylinder assembly converts the uniaxial compression imparted by movement of the piston into a more hydrostatic compression of the sample volume due to deformation of the pressure medium and other soft parts of the assembly. However, decompression is mainly uniaxial after quenching, leading to sample cracking. In order to prevent sample cracking during decompression, a specially designed sample assembly was used, with a low-friction NaCl pressure medium, and a NaCl spacer below the sample volume. With decompression over several days, the redesigned assembly minimized sample cracking considerably. The sample assembly also contained a tapered internal graphite resistance furnace to minimize thermal gradients along the length of the sample volume. Temperature gradients are estimated to be less than 25 °C over the length of the sample volume for the experimental conditions used (Bromiley, unpublished results). The pressure was calibrated against the quartz-coesite and kyanite-sillimanite transitions, as well as the melting point of diopside, and is accurate to within less than ±5% of the stated value. The temperature was measured with a type S thermocouple. No correction for the effects of pressure on thermocouple EMF was applied. Experiments were pressurized to within 90% of the desired run pressure and then heated at 100 °C/min to the run temperature, before being fully pressurized. Run pressures and temperatures were continually monitored and maintained throughout the experiments. The experiments were quenched by switching off the power to

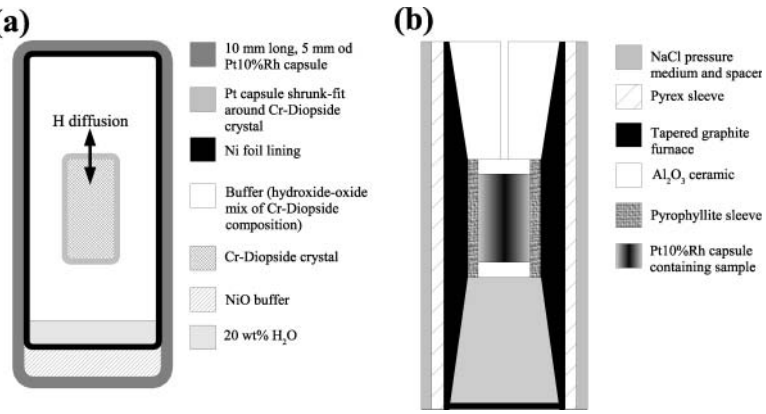

FIGURE 1. Experimental set-up used in annealing experiments (not to scale). (**a**) Cross-section of double capsule. (**b**) Cross-section of piston-cylinder pressure assembly.

the heating circuit. Recovered capsules were weighed and pierced, and then heated and reweighed to check for the presence of water. The capsules were then opened and the inner capsules were recovered. Platinum was removed from around the samples by careful polishing. The samples were recovered relatively crack-free (Fig. 2), and showed no evidence of reaction or degradation.

Infrared spectra were obtained with a Bruker IFS 120 HR high-resolution FTIR spectrometer coupled with a Bruker IR microscope containing all-reflecting Cassegranian optics. The spectrometer contains a permanently aligned Michelson-type interferometer with a 30° angle of incidence to the beam-splitter. Measurements were taken using a tungsten light source, an Si-coated CaF_2 beamsplitter, and a narrow-band MCT detector. Several hundred scans were acquired for each spectrum. The radiation was polarized using a wire-strip polarizer on a KRS-5 substrate. The optics of the microscope were continually purged with H_2O- and CO_2-free, purified air during measurements, and the optics of the spectrometer were kept under vacuum to prevent absorption bands caused by water vapor. Variable apertures in the rear focal plane of the 15× Cassegranian objective were used to obtain spectra from 60 to 200 µm areas. The samples were suspended over large apertures and spectra obtained from crack-free regions. The spectra were obtained using radiation polarized parallel to the **a**, **b**, and **c*** axes of the diopside samples. The water contents were calculated by integrating polarized IR spectra across the region of absorption due to OH dipole vibration (4000–2500 cm^{-1}) after background and thickness corrections were applied. The integrated extinction coefficient of Bell et al. (1995) [7.09(32) per ppm $H_2O \cdot cm^2$] was used in accordance with previous investigations of hydrogen incorporation in diopside. Convergence of determined integral coefficients for diopside means that IR spectroscopy can now be used to accurately determine water contents in diopside (Ingrin and Skogby 2000).

Mössbauer analysis was performed using single crystals of Cr-diopside mounted behind a 2 mm diameter hole drilled into 1 mm thick Pb foil. The crystals were polished to thicknesses of approximately 600 µm, giving an absorber thickness of ~2 mg Fe/cm^2, which is close to the optimum thickness for the Cr-diopside composition (Long et al. 1983). For some measurements a powdered sample was used; this was mounted using cellophane tape in 1 mm diameter holes drilled into 1 mm thick Pb foil.

Mössbauer spectra were recorded at room temperature (293 K) in transmission mode using a constant-acceleration Mössbauer spectrometer with either a nominal 1.85 GBq ^{57}Co source in a 6 µm Rh matrix (conventional source) or a nominal 370 MBq ^{57}Co high specific-activity source in a 12 µm Rh matrix (point source). The velocity scale was calibrated relative to 25 µm α-Fe foil using the positions certified for National Bureau of Standards standard reference material no. 1541; line widths of 0.28 mm/s (conventional source) and 0.36 mm/s (point source) for the outer lines of α-Fe were obtained at room temperature. Further description of the method using a point source (Mössbauer milliprobe) is given in McCammon et al. (1991) and McCammon (1994). The spectra took between 3 and 7 days each to collect. The Mössbauer spectra were fitted using the commercially available fitting program NORMOS written by R.A. Brand (distributed by Wissenschaftliche Elektronik GmbH, Germany).

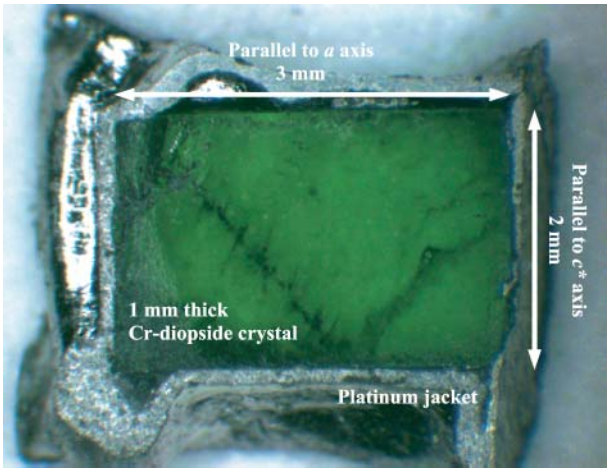

FIGURE 2. The Cr-diopside sample after the annealing experiment. The crystal is still partially surrounded by the Pt "jacket", with the top and bottom of jacket removed by polishing. The crystal was orientated with the **a** axis parallel to the length of the furnace during the experiment.

RESULTS

Kinetics of water dissolution and attainment of equilibrium

Experimental conditions and water contents for all samples are listed in Table 1. A series of annealing experiments were performed at 1.5 GPa and 1100 °C for increasing amounts of time to demonstrate the attainment of equilibrium water contents in annealed samples. Figure 3 shows averaged FTIR spectra (average of 3 spectra using radiation polarized parallel to **a**, **b**, and **c***) obtained from samples annealed at 1.5 GPa for increasing amounts of time. The spectrum from the ambient sample contains 3 absorption bands: one large band at 3646 cm^{-1}, and two smaller bands at 3558 and 3525 cm^{-1}, corresponding to a total of 95 ppm H_2O. All spectra obtained from annealed samples contain an additional absorption band at 3434 cm^{-1}. A very unusual evolution of water contents with time was observed upon annealing. After 48 hours, the water content of the annealed sample was significantly higher than that of the starting material. However, with increasing time the water content of the annealed samples started to decrease slowly. Changing water contents is a function of changing peak heights for the absorption bands at 3646 and 3434 cm^{-1}. No significant changes in peak height for the bands at 3558 and 3525 cm^{-1} were noted. No evidence for diffusion profiles, differences in relative peak height of the absorption bands, or different water contents from different parts of the crystal was noted in any of the samples. Figure 4 shows a plot of run duration against calculated water content for the samples annealed at 1.5 GPa. A general decay law of the form $y = A + B^*\exp(-x/C)$ was fitted to the data, where y is the water content in ppm H_2O by weight and x is experiment duration in hours. Values of 153.41, 178.95, and 68.27 for parameters A, B, and C, respectively, were refined. Using the decay law, equilibrium water contents should be attained at approximately 250 hours. The calculated water content of the sample annealed for over 300 hours (CrDi8) is slightly lower than expected. For this sample the Ni-NiO oxygen-buffer was exhausted during the experiment, and the low water content is probably due to disequilibrium (i.e., change in oxygen fugacity). The calculated water content of the sample annealed for 193 hours is within the experimental error of the equilibrium value. Therefore, times of approximately 200 hours were used in subsequent annealing experiments, with slightly longer times

TABLE 1. Experimental conditions and calculated water contents for high-pressure annealing experiments

Run no.	Pressure (GPa)	Temperature (°C)	Duration (h)	O atom buffer	Water content (ppm H_2O)
CrDi1	–	–	–	–	95 ± 4
CrDi2	1.5	1100	48	Ni-NiO	242 ± 11
CrDi5	1.5	1100	98	Ni-NiO	196 ± 9
CrDi11	1.5	1100	193	Ni-NiO	164 ± 7
CrDi8	1.5	1100	317.5	Ni-NiO	148 ± 7
CrDi7	0.5	1000	257	Ni-NiO	130 ± 6
CrDi9	1.0	1000	205	Ni-NiO	145 ± 7
CrDi10	2.5	1100	197	Ni-NiO	202 ± 9
CrDi6	3.0	1100	160	Ni-NiO	215 ± 10
CrDi12	4.0	1100	188	Ni-NiO	229 ± 10
CrDi13	1.5	1100	196	Fe-FeO	446 ± 20

Note: CrDi1 is the untreated sample.

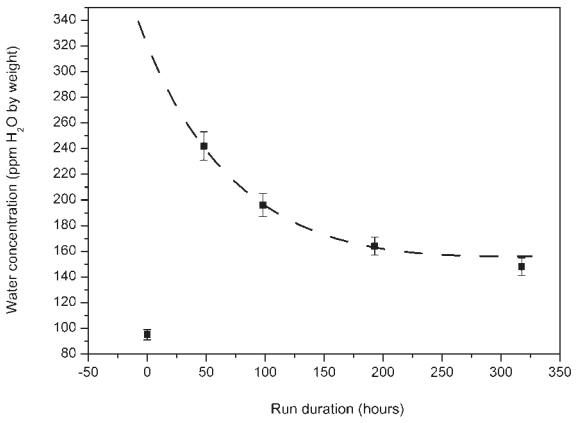

FIGURE 3. Averaged polarized FTIR spectra for Cr-diopside samples annealed at 1.5 GPa and 1100 °C under Ni-NiO buffer conditions for increasing amounts of time (offset vertically). Experiment durations and water contents for each sample are given.

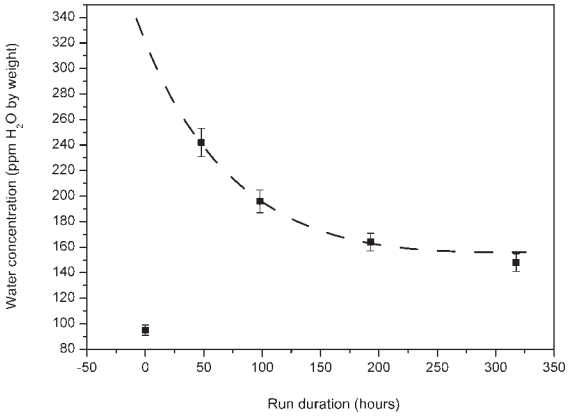

FIGURE 4. Plot of run duration vs. water content for Cr-diopside samples annealed at 1.5 GPa. The broken line is a fit of a simple exponential decay law to the sample water concentrations with increasing annealing times.

for lower pressure experiments. Whether the state of the samples obtained during these experiments corresponds to a stable or a metastable equilibrium will be discussed below.

Water solubility as a function of pressure

Experiments were performed from 0.5 to 4.0 GPa and 1000 to 1100 °C to determine the solubility of water in the Cr-diopside sample as a function of pressure. Details of all experiments are given in Table 1. Typical polarized spectra from an annealed sample are shown in Figure 5. All absorption bands exhibit some degree of anisotropy. Averaged spectra from samples annealed at pressures from 0.5 to 4.0 GPa are shown in Figure 6. No changes in peak position or in the number of absorption bands were noted as a function of increasing pressure. However, a small increase in peak height for all absorption bands, especially the two prominent bands at 3646 and 3434 cm^{-1} is noted with increasing pressure, corresponding to a small increase in the calculated water contents. The pressure dependence of water solubility in NAMs is governed by water fugacity and the volume change,

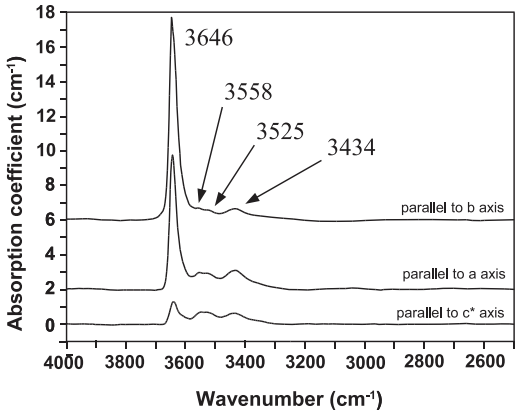

FIGURE 5. Polarized FTIR spectra for a Cr-diopside sample annealed at 1.0 GPa and 1000 °C for 205 hours under Ni-NiO buffer conditions.

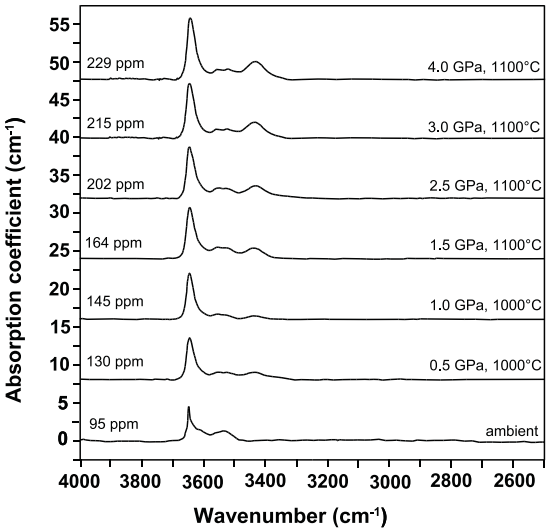

FIGURE 6. Averaged polarized FTIR spectra for Cr-diopside samples annealed under Ni-NiO buffer conditions at pressures from 0.5 to 4.0 GPa (offset vertically with increasing pressure). The experimental conditions and water contents for each sample are given.

ΔV_s, of the host structure due to incorporation of OH groups (Lu and Keppler 1997). This relationship can be expressed in terms of the general solubility equation

$$c_{OH} = A\, f_{H_2O}{}^{n} \exp(-P\Delta V_s/RT) \quad (1)$$

(where c_{OH} is water solubility, A is a temperature-dependent constant, f_{H_2O} is water fugacity, P and T are run pressure and temperature, and R is the gas constant). Fitting this equation to solubility data for different values of n indicates whether hydrogen is incorporated as isolated hydroxyl groups, as hydroxyl pairs, or as more complicated hydroxyl clusters (Kohlstedt et al. 1996; Lu and Keppler 1997; Rauch and Keppler 2002). Figure 7 shows two possible fits of the general solubility law to the data. Despite the limited pressure range of the annealing experiments, a visibly better fit is obtain for a value of $n = 0.5$ (with values of 2.15 ppm/$bar^{0.5}$ and 7.43 cm^3/mol for A and ΔV_s, respectively).

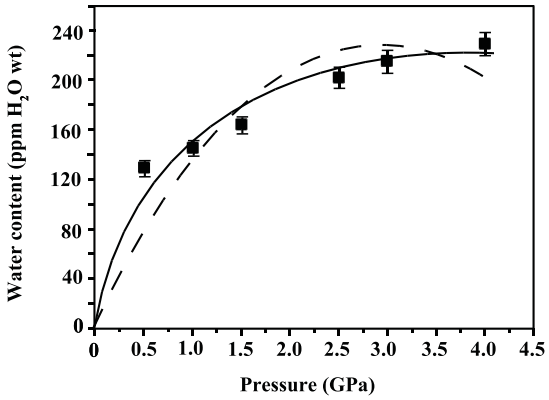

FIGURE 7. Pressure dependence of water solubility in annealed Cr-diopside at 1000 to 1100 °C under Ni-NiO buffer conditions. The error bars for calculated water contents represent error on value of integrated absorption coefficient used. Two fits of the general solubility law $c_{H_2O} = A\, f_{H_2O}{}^{n} \exp(-P\Delta V/RT)$ for values of $n = 1$ (broken line) and $n = 0.5$ (solid line) are shown.

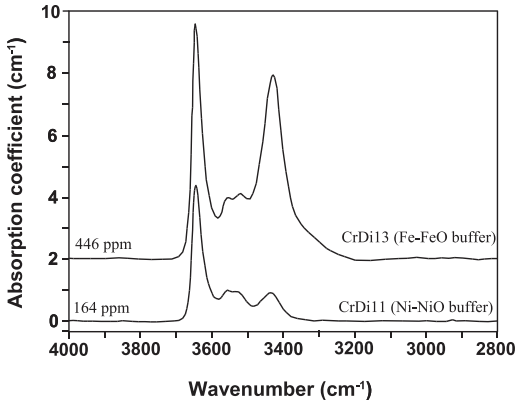

FIGURE 8. Averaged polarized FTIR spectra for Cr-diopside samples annealed at 1.5 GPa and 1100 °C for approximately 200 hours under Ni-NiO and Fe-FeO buffer conditions.

Differences between the calculated water contents for annealed samples and equilibrium water contents (as discussed in the previous section) are probably within the errors of the calculations, and are unlikely to have a marked influence on the fit of the solubility law. The fit of the solubility law indicates that water solubility in the Cr-diopside sample is proportional to the square root of water fugacity, implying that water is incorporated in the structure as isolated hydroxyl groups. In contrast, Rauch and Keppler (2002) found that water was incorporated in pure, water-saturated enstatite as hydroxyl pairs, possibly as a direct substitution for Mg^{2+} cations.

Effect of oxygen fugacity on water solubility

An additional annealing experiment was performed at 1.5 GPa and 1100 °C using an Fe-FeO O atom buffer to determine the effect of oxygen fugacity on water solubility in the Cr-diopside sample. The same experimental set-up as shown in Figure 1a was used, but with an outer Fe capsule, and FeO powder present inside the capsule (in place of the NiO powder). Figure 8 shows a comparison of averaged spectra from samples annealed under Fe-FeO and Ni-NiO buffer conditions. All absorption bands in the Fe-FeO buffered sample are considerably larger than in the Ni-NiO buffered sample. The bands at 3646, 3558, and 3525 cm^{-1} exhibit an approximate doubling in peak height between the samples. In contrast, the band at 3434 cm^{-1} shows a more than fourfold increase in peak height. Changes in peak height are reflected in an almost threefold increase in calculated water contents between the two samples (Table 1). The effect of buffer conditions on water solubility in the Cr-diopside sample suggests that hydrogen incorporation may be linked to reduction of Fe^{3+} at cation sites in the diopside structure; e.g.,

$$2Fe^{3+}_{diopside} + 2O^{2-}_{diopside} + H_{2\ gas} = 2Fe^{2+}_{diopside} + 2OH^{-}_{diopside} \quad (2)$$

Different changes in relative peak heights for different absorption bands in IR spectra from the Cr-diopside sample could imply that the absorption bands are related to hydrogen incorporation mechanisms associated with different cation sites in the structure.

Incorporation of hydrogen via mechanism 2 would imply a 1:1 ratio between the number of OH groups incorporated and the number of Fe^{3+} cations reduced to Fe^{2+} during annealing. In order to check this, selected samples annealed at 1.5 GPa and the starting material were analyzed using Mössbauer spectroscopy.

The spectrum of Cr-diopside is dominated by a quadrupole doublet, where the relative areas of the doublet components are either equal due to random crystallite orientation (polycrystalline spectra, e.g., Fig. 9a), or unequal due to preferred orientation (single-crystal spectra, Figs. 9b–d). The asymmetry of the component relative areas depends on the orientation of the single crystal. In order to minimize the effects of preferred orientation of the single crystals, we simply allowed the area ratio between the two doublet components to vary. Starting with spectra from polycrystalline samples, we fitted two quadrupole doublets with the conventional constraints of equal component areas and widths. We then applied the same fitting model, but with the constraint of equal component areas for the dominant doublet removed, to the spectra obtained from single crystals. We were able to measure both polycrystalline and single crystal spectra from one sample (CrDi1; Figs. 9a and 9b), and verify that the same hyperfine parameters were obtained for each. We calculated $Fe^{3+}/\Sigma Fe$ for each sample based on the relative areas, where effects due to differing recoil-free fractions and thickness effects were judged to be within the uncertainty of the data. Errors were estimated based on statistical errors of the fitting model, and uncertainties in the model itself (e.g., line shape, asymmetry in Fe^{3+} absorption). Table 2 gives details of samples analyzed and the results of Mössbauer spectroscopy to quantify Fe^{3+}/Fe_{total} ratios. Figure 10 shows a graph of calculated water content for the samples against Fe^{3+}/Fe_{total}. As expected, there is a noticeable trend of increasing water content with decreasing Fe^{3+}/increasing Fe^{2+} content. Using information on the composition of the Cr-diopside samples, it is possible to directly calculate the number of additional OH groups incorporated and the number of Fe^{3+} cations converted to Fe^{2+} for the annealed samples (Table 3). For all samples except CrDi13 the increase in OH per formula unit is approximately equal to the increase in Fe^{2+} per formula

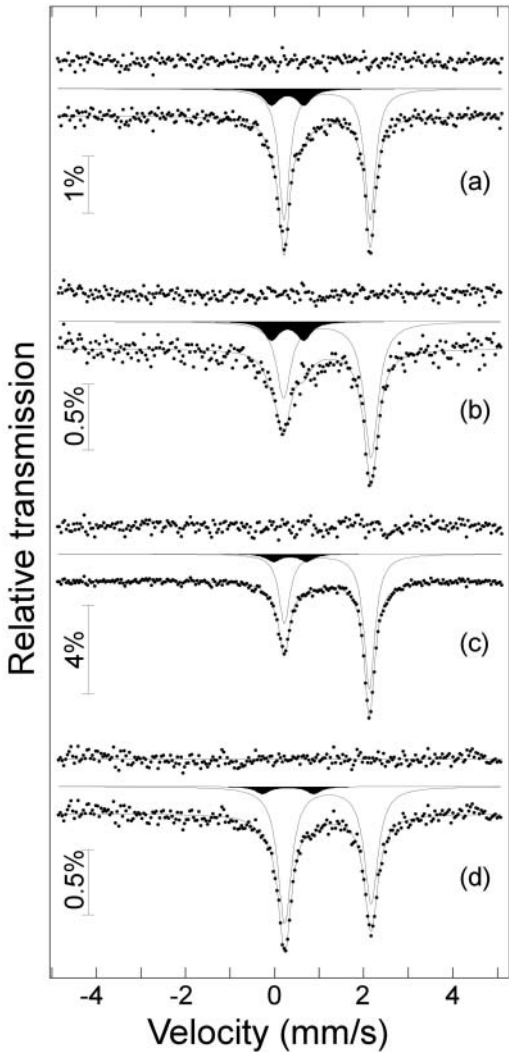

FIGURE 9. Room temperature Mössbauer spectra of Cr-diopside: (**a**) polycrystalline CrDi1 (starting material); (**b**) single-crystal CrDi1 (starting material); (**c**) single-crystal CrDi11 (annealed for 193 h at Ni-NiO buffer); (**d**) single-crystal CrDi13 (annealed for 193 h at Fe-FeO buffer). The experimental data and fitted curve, subspectra and residual, are shown for each sample. The shaded and unshaded doublets correspond to Fe^{3+} and Fe^{2+}, respectively. The top two spectra demonstrate that polycrystalline and single crystal forms of the same sample give the same $Fe^{3+}/\Sigma Fe$ values, as indicated by the relative areas.

unit. For sample CrDi13, which was buffered under Fe-FeO conditions, the calculated increase in OH is double that of Fe^{2+}. However, within the considerable uncertainties of the calculation and uncertainties in determination of water contents and Fe^{3+}/Fe_{total} ratios, it can be concluded that the main mechanism for hydrogen incorporation in the Cr-diopside samples during annealing is reduction of Fe^{3+}.

DISCUSSION

Mechanism of hydrogen incorporation in diopside

Differences in peak height between the four absorption bands in the IR spectra for the Cr-diopside samples as a function of water fugacity (i.e., pressure), oxygen fugacity and experiment duration, and differences in absorption band anisotropy with direction of polarization of radiation, imply that there are four distinct mechanisms for hydrogen incorporation in the annealed samples. In silicates, structurally incorporated hydrogen atoms are associated with specific O atom sites in the host lattice. Nakamoto et al. (1955) noted a correlation between OH-stretching frequencies and O-O distances in a large number of minerals. Using the recent improved calibration of this correlation by Libowitzky (1999), it is possible to use OH-stretching frequencies determined from IR data and information on absorption band anisotropy to elucidate potential hydrogen incorporation mechanisms. This approach assumes that vibration of OH dipoles is approximately co-linear with O-O bonds, which appears to be true except in certain limiting examples, such as hydrogen incorporation in garnet via the hydrogrossular mechanism (Lager et al. 1989). Using this approach, it is possible to tentatively assign the two most prominent absorption bands in the IR spectra. The band at 3646 cm^{-1} is probably due to hydrogen incorporation onto the O2 site in the diopside structure, with vibration of the OH dipole in the direction of a nearby O3 site (i.e., along the edge of an M2 polyhedral site). This mechanism (1) was previously proposed by Beran (1976) to account for prominent absorption bands seen in IR spectra for natural diopside. Two additional mechanisms could both explain the absorption band at 3434 cm^{-1}. Mechanism 2 involves hydrogen incorporation onto the O2 site and vibration of the OH dipole in the direction of the O1 site, along a shared M1–M2 polyhedral edge. Mechanism 3 involves hydrogen incorporation onto the O2 site with vibration of the OH dipole in the direction of another O2 site along the edge of an M1 octahedron. Hydrogen incorporation onto the O2 site in pyroxenes with the C2/c structure would be favored because, on the basis of site potential calculations (Smyth 1989), this site is underbonded. This is reflected in calculated values for the sum of the Pauling's bond strength at the anion sites in the Cr-diopside composition used in this study: 1.91, 1.58, and 2.246 for the O1, O2, and O3 sites, respectively. It was not possible to assign the two small absorption bands at 3558 and 3525 cm^{-1} because

TABLE 2. Fe^{3+}/Fe_{total} ratios, determined by Mössbauer spectroscopy, for Cr-diopside samples annealed at 1.5 GPa and 1100 °C for various times and under different O atom buffer conditions

Sample	Buffer	Run duration (h)	$Fe^{3+}/\Sigma Fe$	ppm H_2O	notes
CrDi1	–	ambient	14 ± 3	95	2nd value for
			15 ± 4		powdered sample
CrDi2	Ni-NiO	48	5 ± 3	242	
CrDi5	Ni-NiO	98	14 ± 6	196	Poor spectral resolution
CrDi11	Ni-NiO	193	9 ± 3	164	
CrDi13	Fe-FeO	193	6 ± 3	446	

TABLE 3. Changes in number of OH groups incorporated, and change in number of Fe^{3+} to Fe^{2+} pfu in Cr-diopside during annealing experiments at 1.5 GPa

Sample	OH pfu	Increase in OH pfu	Minimum increase in Fe^{2+} pfu	Maximum increase in Fe^{2+} pfu
CrDi1	0.0024	0	–	–
CrDi2	0.0060	0.0036	0.0025	0.0047
CrDi5	0.0048	0.0024	0	0.0025
CrDi11	0.0040	0.0016	0.0011	0.0032
CrDi13	0.0110	0.0086	0.0022	0.0043

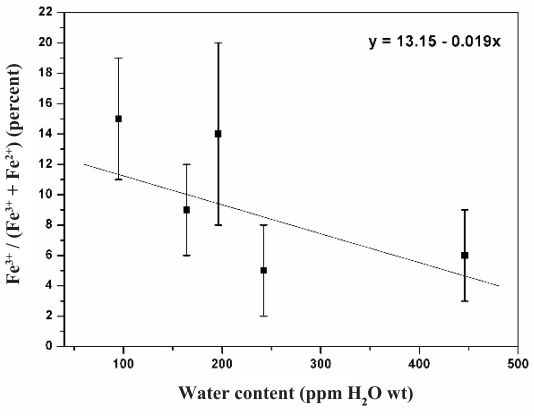

FIGURE 10. Plot of Fe^{3+}/Fe_{total} vs. water content for samples annealed at 1.5 GPa for different amounts of time and under different O atom buffers. A linear line of best fit (equation given) is fitted to the data.

band anisotropy was not easily determined. However, several additional incorporation mechanisms involving the underbonded O2 site or the O1 site could account for these bands. Hydrogen incorporation onto the O3 site in the diopside structure is least likely because it is a silicate bridging O atom (the sum of the Pauling bond strengths at the O3 site is significantly higher than 2.00). All possible hydrogen incorporation mechanisms involve O-O bonds around either M1 or M2 polyhedral sites. O-O distances around tetrahedral sites in the diopside structure are too short to account for any of the absorption bands seen in the IR spectra.

Differences between the nature of mechanism 1 and mechanisms 2 and 3 are consistent with the differing effect of oxygen fugacity on peak heights for the two absorption bands at 3646 and 3434 cm^{-1}. The band at 3646 cm^{-1} shows a doubling in peak height between the Ni-NiO and Fe-FeO buffered samples, whilst the band at 3434 cm^{-1} shows a fourfold increase in peak height. Differences in relative peak height between the two samples are due to differences in the amount of reduction of Fe^{3+} at cation sites. This may suggest that the two bands are due to H incorporation onto O sites associated with two different cation sites. Mechanism 1 implies H associated with the M2 site. Mechanisms 2 and 3 involve either H associated with M1 and M2, or only M1 sites. Differences in changing peak height could therefore imply differences in the amount of Fe^{3+} reduction at the two polyhedral sites in the diopside structure. However, this simple interpretation implies that a significant amount of Fe^{3+} is present at both cation sites in the diopside structure. The ionic radius of Fe^{3+} is considerably smaller than the radius of Mg^{2+}, and it is highly unlikely that a significant fraction of Fe^{3+} would substitute for the large Ca^{2+} ion at the M2 site. Rather, it is generally assumed that in clinopyroxenes, virtually all Fe^{3+} is at the M1 site. However, there are two possible mechanisms that could charge balance the Fe^{3+} cation. Either Fe^{3+} at M1 is charge balanced by Na^{+} at M2 or Fe^{3+} at M1 is coupled to Al^{3+} at the tetrahedral (T) site. According to the bulk composition of the diopside crystal studied, both mechanisms are possible. Reduction of Fe^{3+} in the diopside samples could therefore be described by the following equations:

$$Fe^{3+}(M1)\ Na^{+}(M2) + 1/2\ H_2 = Fe^{2+}(M1)\ Na^{+}H^{+}(M2) \quad (3)$$

$$Fe^{3+}(M1)\ Al^{3+}(T) + 1/2\ H_2 = Fe^{2+}H^{+}(M1)\ Al^{3+}(T) \quad (4)$$

$$Fe^{3+}(M1)\ Al^{3+}(T) + 1/2\ H2 = Fe^{2+}(M1)\ Al^{3+}H^{+}(T) \quad (5)$$

Equation 3 implies that hydrogen is required for charge balancing the M2 site. Accordingly, the band at 3646 cm^{-1} could be tentatively assigned to the reduction of Fe^{3+} charge balanced by Na^{+} on M2. In contrast to this, Equation 4 suggests that hydrogen should be incorporated close to M1. Accordingly, the band at 3434 cm^{-1} may be due to the reduction of Fe^{3+} charge balanced by Al^{3+} at the tetrahedral site.

Attainment of equilibrium

The annealing experiments highlight the importance of Fe^{3+} reduction at cation sites in providing a local charge-balancing mechanism. In fact, experiments conducted using different oxygen buffers suggest that the only significant change that occurs during the annealing experiments is the Fe^{3+}/Fe^{2+} ratio. Therefore, full re-equilibration of the defect chemistry of the samples is not attained. In perfect equilibrium, the oxidation state of Fe in diopside should depend only on oxgyen fugacity, not on water fugacity. The observed variation of Fe redox state even in samples exposed to the same oxygen fugacity buffered by Ni-NiO therefore implies that the equilibrium state obtained during annealing is only metastable. For attaining stable equilibrium, cations and vacancies would have to diffuse throughout the entire mm-sized sample. According to available diffusion coefficients for diopside (e.g., Brady and McCallister 1983), this is not realistic for the temperatures and durations of our experiments. For this reason, the value of ΔV_s from the fit in Equation (1) may not be physically meaningful.

Fe^{3+} reduction is probably the most important mechanism for hydrogen diffusion in pyroxenes (Ingrin and Skogby 2000), but other types of point defects such as cation vacancies or lower valency substitutions into cation sites could locally charge-balance hydrogen incorporation (for example, Na^{+} at the M2 site). However, if the main mechanism for hydrogen loss from UHP pyroxenes during exhumation is oxidation, then the effect of the long-duration annealing experiments (Fe^{3+} reduction and concurrent hydrogen incorporation) is probably to re-saturate the Cr-diopside samples and thereby provide a measure of the original water content. The Cr-diopside samples used in these high-pressure experiments are from a hydrothermal deposit, and have therefore probably undergone late stage oxidation, and concurrent dehydrogenation, in the crust. The hypothesis that annealing merely reverses the process of oxidation and hydrogen loss is further supported by the effect of water fugacity on water solubility. The fit of the solubility law to the experimental data on water solubility given in Figure 7 suggests that even if the pressure were increased significantly, there would be no further increase in water solubility, and that at a certain pressure, water solubility in the Cr-diopside sample would become independent of changes in water fugacity. The amount of water incorporated

in the samples is probably largely a function of the original composition and defect structure. Furthermore, the amount of water incorporated in the samples is markedly different from that which could be calculated by simply assuming that all Fe^{3+} could be replaced by Fe^{2+} and H^+.

One further interesting feature to note from the IR spectra for annealed and unannealed samples is the ratio in peak height between the absorption bands at 3434 and 3646 cm^{-1}. For all samples annealed under Ni-NiO buffer conditions (Fig. 6), this ratio appears to be constant, implying that it is independent of water fugacity. However, the ratio appears to change significantly as a function of O atom fugacity (Fig. 8). The ratio of peak heights of the 3434 to 3646 cm^{-1} bands could, therefore, provide a measure of the redox state "frozen in" to the sample. Rauch and Keppler (2002) noted a similar, although much smaller, increase in the ratio of peak heights of absorption bands at approximately 3400 and 3600 cm^{-1} in spectra obtained from natural, aluminous enstatite annealed under Fe-FeO compared to Ni-NiO buffer conditions. If water is lost from pyroxenes as H_2, resulting in oxidation of the sample, then the relative ratio of peak heights for bands at approximately 3400 and 3600 cm^{-1} could provide a measure of how much water loss has taken place in natural samples during ascent into the crust. This proposition is, of course, consistent with the absence of the 3434 cm^{-1} band in IR spectra obtained from the Cr-diopside starting material.

To test whether the ratio of the 3434 to 3646 cm^{-1} band peak height could provide a measure of the internal redox state of the Cr-diopside sample, a further heating experiment was performed. A small (unoriented) piece of the sample annealed under Fe-FeO buffer conditions (CrDi13) was placed in a microscope heating stage of the type described by Zapunnyy et al. (1989) and heated in air at 1000 °C for increasing amounts of time. Unpolarized FTIR spectra were obtained at various intervals after the sample had cooled to room temperature (Fig. 11). As expected, oxidation of the sample is concurrent with water loss, as predicted by Equation (2), and after 4 hours, the sample is almost dry. Table 4 gives the absolute peak heights of the absorption bands at 3434 and 3646 cm^{-1}, as well as the peak ratio. This ratio decreases with decreasing water content, implying that the ratio could potentially be used to provide a measure of water loss from mantle pyroxenes during ascent or exhumation.

Kinetics of water dissolution

One of the most puzzling observations of this study is the fact that upon annealing, the water content of the samples first sharply increases and then slowly decreases to a metastable equilibrium value. Inspection of Figure 3 shows that the band at 3646 cm^{-1} is initially very sharp. Upon annealing, this band broadens significantly while the water content of the sample decreases. This broadening of the band suggests that the decrease in water content with time is related to some disordering process.

Hydrogen probably diffuses into the crystal very rapidly and causes a local reduction of Fe^{3+}. As discussed above, the mechanism responsible for the increase of the 3646 cm^{-1} band is probably

$$Fe^{3+}(M1)\ Na^{+}(M2) + 1/2\ H_2 = Fe^{2+}(M1)\ Na^{+}H^{+}(M2). \quad (3)$$

Therefore, initially the proton is close to a Na^+ ion in an M2 site next to an M1 site occupied by Fe^{2+}. However, once Fe^{3+} is reduced to Fe^{2+}, there is no need for Fe^{2+} and Na^+H^+ to stay next to each other. With time, Fe^{2+}-Mg^{2+} disordering will occur at M1, leading to a range of different environments around the OH group and therefore causing a broadening of the 3646 cm^{-1} band. Moreover, Fe^{2+} is considerably more electronegative than Mg^{2+}. Accordingly, when Fe^{2+} is replaced by Mg^{2+}, the electron density at the O2 atom will increase. This implies that the O2 atom becomes less underbonded and therefore the capacity of the pyroxene structure to incorporate water decreases. Using existing data on rates of cation diffusion in clinopyroxenes (Brady and McAllister 1983), it is possible to calculate the expected times of Fe^{2+}-Mg^{2+} disordering under the experimental conditions used. At 1100 °C and 100 hours duration, the estimated depths of diffusion are in the order of 700 Å, which is hundreds of times the size of the unit cell. On the basis of these results, cation diffusion in the samples will certainly occur during the annealing process, consistent with the above hypothesis.

For experiments performed at 1.5 GPa for varying amounts of times, it was demonstrated that metastable equilibrium values for water contents should be achieved after 250 hours annealing. However, in experiment CrDi8, which was annealed for over 300 hours, the calculated water content was slightly below the metastable value. During this experiment, the Ni-NiO buffer was

TABLE 4. Absolute peak heights (corrected for 1 cm thickness of sample) and peak height ratios for the two main IR absorption bands in sample CrDi13 after heating in air at 1000 °C for increasing amounts of time

Time heated at 1000 °C (hours)	Peak height (cm^{-1}) of band at 3646 cm^{-1}	Peak height (cm^{-1}) of band at 3434 cm^{-1}	Peak height ratio: 3434/3646
Before heating	6.94	1.93	0.28
0.5	5.42	1.30	0.24
1	4.67	0.79	0.17
2	3.69	0.24	0.03
3	1.73	0.09	0.01
4	0.48	0.000	0.00

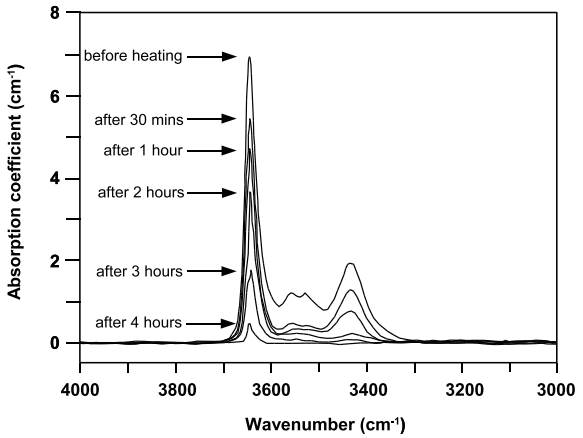

FIGURE 11. Unpolarized FTIR spectra (background and thickness corrected) for sample CrDi13 after heating in air at 1000 °C for increasing amounts of time.

exhausted, and so the oxygen fugacity was unconstrained during the latter part of the run time. A lower than expected water content would be consistent with an increase in oxygen fugacity after exhaustion of the buffer, leading to oxidation of Fe^{2+} at the M1 site and concurrent H loss. Buffer conditions in the piston-cylinder assembly used in these experiments are estimated to be slightly more oxidizing than Ni-NiO, which would explain the lower water content of sample CrDi8.

Applicability of results

Measured water contents in the annealed samples are consistent with the highest values reported for Cr-diopsides from mantle xenoliths, where the oxidation state is likely to lie between Ni-NiO and Fe-FeO buffer conditions (Ingrin and Skogby 2000). This is consistent with the hypothesis that the annealing technique reverses the main mechanism for hydrogen loss from the samples, and implies that this technique could be used to determine equilibrium water contents in other mantle samples. This could be particularly useful in determining water solubility in complex solid-solutions such as omphacite, which are not amenable to investigation using simple synthesis experiments.

ACKNOWLEDGMENTS

The authors thank H. Schulze for sample preparation, G. Herrmannsdörfer, and H. Fischer for technical assistance with, and manufacturing of, components for the piston-cylinder apparatus, and D. Krauße for assistance with the EMPA. This manuscript benefited from prompt and thorough reviews by H. Skogby and S.C. Woods. The work was financially supported by the EU Hydrospec network (Improving Human Potential Programme).

REFERENCES CITED

Bell, D.R. and Rossman, G.R. (1992) Water in the Earth's mantle: the role of nominally anhydrous minerals. Science, 255, 1391–1397.

Bell, D., Ihinger, P., and Rossman, G.R. (1995) Quantitative analysis of trace OH in garnet and pyroxenes. American Mineralogist, 80, 465–474.

Beran, A. (1976) Messung des Ultrarot-Pleochroismus von Mineralen. XIV. Der Pleochroismus der OH-Streckfrequenz in Diopsid. Tschermaks Mineralogische und Petrographische Mitteilungen, 23, 79–85.

Bolfan-Casanova, N., Keppler, H., and Rubie, D.C. (2000) Water partitioning between nominally anhydrous minerals in the MgO-SiO_2-H_2O system up to 24 GPa: implications for the distribution of water in the Earth's mantle. Earth and Plantary Science Letters, 182, 209–221.

Brady, J.B. and McCallister, R.H. (1983) Diffusion data for clinopyroxenes from homogenization and self-diffusion experiments. American Mineralogist, 68, 95–105.

Bromiley, G. and Keppler, H. (2004) An experimental investigation of hydroxyl solubility in jadeite and Na-rich pyroxenes. Contributions to Mineralogy and Petrology, 147, 189–200.

Cameron, M. and Papike, J. (1981) Structural and chemical variations in pyroxenes. American Mineralogist, 66, 1–50.

Gasparik, T. (1986) Experimental study of subsolidus phase relations and mixing properties of clinopyroxene in the silica-saturated system CaO-MgO-Al_2O_3-SiO_2. American Mineralogist, 71, 686–693.

Green, H., Dobrzhinetskaya, L., and Bozhilov, K. (2000) Mineralogical and experimental evidence for very deep exhumation from subduction zones. Journal of Geodynamics, 30, 61–76.

Hercule, S. and Ingrin, J. (1999) Hydrogen in diopside: diffusion, kinetics of extraction-incorporation, and solubility. American Mineralogist, 84, 1577–1587.

Ingrin, J. and Skogby, H. (2000) Hydrogen in nominally anhydrous upper-mantle minerals: concentration levels and implications. European Journal of Mineralogy, 12, 543–570.

Katayama, I. and Nakashima, S. (2003) Hydroxyl in clinopyroxene from the deep subducted crust: evidence for H_2O transport into the mantle. American Mineralogist, 88, 229–234.

Kohlstedt, D., Keppler, H., and Rubie, D.C. (1996) Solubility of water in the α, β and γ phases of $(Mg,Fe)SiO_4$. Contributions to Mineralogy and Petrology, 123, 345–357.

Lager, G.A., Armbruster, T., Rotella, F.J., and Rossman, G.R. (1989) OH substitution in garnets: X-ray and neutron diffraction, infrared, and geometric-modelling studies. American Mineralogist, 74, 840–851.

Libowitzky, E. (1999) Correlation of O-H stretching frequencies and O-H···O hydrogen bond lengths in minerals. Monatshefte für Chemie, 130, 1047–1059.

Long, G.L., Cranshaw, T.E., and Longworth, G. (1983) The ideal Mössbauer effect absorber thickness. Mössbauer Effect Reference and Data Journal, 6, 42–49.

Lu, R. and Keppler, H. (1997) Water solubility in pyrope to 100 kbar. Contributions to Mineralogy and Petrology, 129, 35–42.

Malinovskaya, E., Doroshev, A., Bulatov, V., and Bray, G. (1991) Clinopyroxenes of $CaMgSi_2O_6$-$CaAl_2SiO_6$-$Ca_{0.5}AlSi_2O_6$ series in association with anorthite, quartz, coesite and garnet. Geokhimiya, 2, 216–226.

McCammon, C.A. (1994) A Mössbauer milliprobe: Practical considerations. Hyperfine Interactions, 92, 1235–1239.

McCammon, C.A., Chaskar, V., and Richards, G.G. (1991) A technique for spatially resolved Mössbauer spectroscopy applied to quenched metallurgical slags. Measurement Science and Technology, 2, 657–662.

Nakamoto, K., Margoshes, M., and Rundle, R. (1955) Stretching frequencies as a function of distances in hydrogen bonds. Journal of the American Chemical Society, 77, 6480–6486.

Rauch, M. and Keppler, H. (2002) Water solubility in orthopyroxene. Contributions to Mineralogy and Petrology, 143, 525–536.

Rossi, G., Smith, D., Ungaretti, L., and Domeneghetti, M. (1983) Crystal-chemistry and cation ordering in the system diopside-jadeite: a detailed study by crystal structure refinement. Contributions to Mineralogy and Petrology, 83, 247–258.

Schmädicke, E. and Müller, W. (2000) Unusual exsolution phenomena in omphacite and partial replacement of phengite by phlogopite + kyanite in an eclogite from the Erzgebirge. Contributions to Mineralogy and Petrology, 139, 629–642.

Schmidt, M. (1993) Phase-relations and compositions in tonalite as a function of pressure - an experimental study at 650 °C. American Journal of Science, 10, 1011–1060.

Skogby, H., Bell, D.R., and Rossman, G.R. (1990) Hydroxide in pyroxene: variations in the natural environment. American Mineralogist, 75, 764–774.

Smyth, J. (1989) Electrostatic characterization of oxygen sites in minerals. Geochimica et Cosmochmica Acta, 53, 1101–1110.

Smyth, J., Bell, D., and Rossman, G. (1991) incorporation of hydroxyl in upper-mantle clinopyroxenes. Nature, 351, 732–735.

Stalder, R. and Skogby, H. (2003) Hydrogen diffusion in natural and synthetic orthopyroxene. Physics and Chemistry of Minerals, 30, 12–19.

Terry, M., Bromiley, G.D., and Robinson, P. (2003) Determination of equilibrium water content and composition of omphacitic pyroxene in a UHP kyanite-eclogite, Western Norway. Geophysical Research Abstracts, 5, 08698.

Withers, A.C., Wood, B.J., and Carroll, M.R. (1998) The OH content of pyrope at high pressure. Chemical Geology, 147, 161–171.

Woods, S., Mackwell, S., and Dyar, D. (2000) Hydrogen in diopside: diffusion profiles. American Mineralogist, 85, 480–487.

Zapunnyy, S., Sobolev, A., Bogdanov, A., Slutsky, A., Dmitriev, L., and Kunin, L. (1989) An apparatus for high-temperature optical research with controlled oxygen fugacity. Geochemistry International, 26(2), 120–128.

Zhang, R. and Liou, J. (1999) Exsolution lamellae in minerals from ultrahigh-pressure rocks. International Geology Review, 41, 981–993.

Zhang, R., Liou, J., Ernst, W., Coleman, R., Sobolev, N., and Shatsky, V. (1997) Metamorphic evolution of diamond-bearing and associated rocks from the Kokchetav Massif, northern Kazakhstan. Journal of Metamorphic Geology, 15, 479–496.

MANUSCRIPT RECEIVED SEPTEMBER 1, 2003
MANUSCRIPT ACCEPTED JANUARY 22, 2004
MANUSCRIPT HANDLED BY ALISON PAWLEY